ARTICLE IN PRESS

ELSEVIER

Journal of Quantitative Spectroscopy & Radiative Transfer ▮▮▮ (▮▮▮▮) ▮▮▮–▮▮▮

Journal of Quantitative Spectroscopy & Radiative Transfer

www.elsevier.com/locate/jqsrt

Assembly of full-spectrum k-distributions from a narrow-band database; effects of mixing gases, gases and nongray absorbing particles, and mixtures with nongray scatterers in nongray enclosures

Michael F. Modest*, Robert J. Riazzi

Department of Mechanical Engineering, Pennsylvania State University, 301C Reber Building, University Park, PA 16802, USA

Received 22 July 2003; accepted 13 March 2004

Abstract

Full-spectrum k-distributions provide great accuracy combined with outstanding numerical efficiency for the evaluation of radiative transfer in absorbing-emitting molecular gases, but they do have several shortcomings: (1) It is difficult to assemble k-distributions for gas mixtures from precalculated full-spectrum k-distributions of individual gas species (i.e., without calculating the mixture k-distribution directly from the HITRAN/HITEMP database), (2) it is impossible to assemble k-distributions for a gas mixed with nongray absorbing particles (such as soot) from gas-only full-spectrum k-distributions, and (3) like all global models, full-spectrum k-distributions cannot accommodate nongray scattering behavior and/or nongray wall reflectances. In the present paper we show how these restrictions can be relaxed by (1) assembling full-spectrum k-distributions for a gas mixture from a narrow-band k-distribution database created for individual gas species, (2) by assembling gas and nongray absorbing particle mixture full-spectrum k-distributions from the same narrow-band database, and finally (3) by showing how a group of part-spectrum k-distributions can be generated from the same database to accommodate nongray scattering and nongray walls.

Keywords: Gas radiation; k-distributions; Gas mixtures

1. Introduction

Line-by-line (LBL) calculations can most accurately predict the radiative transfer in participating gaseous media, but are often not practical because of the large computational effort they require.

* Corresponding author. Tel.: +1-814-863-8682; fax: +1-814-863-8682.
E-mail address: mfm6@psu.edu (M.F. Modest).

0022-4073/$ - see front matter © 2004 Elsevier Ltd. All rights reserved.
doi:10.1016/j.jqsrt.2004.03.007

For a small spectral interval (i.e., a range over which the Planck function is nearly constant), in a homogeneous medium (i.e., the absorption coefficient κ_η is not a function of spatial location), the absorption coefficient may be reordered into a monotonic k-distribution, which yields exact results in a small fraction of the time required for LBL calculations [1,2]. However, this model, like other narrow band models, is not well suited for inhomogeneous media. One of two different, but related, assumptions of either a correlated or a scaled absorption coefficient may be adopted to overcome this shortcoming. Extensive information is available as to the validity of each [1,3,4].

More recently methods have been developed that allow the concept of reordering the absorption coefficient to be applied to the entire spectrum. Modest and Zhang [5] and Modest [6] have shown how a k-distribution may be developed for the entire spectrum and applied to problems with inhomogeneous media by assuming that the absorption coefficient is either scaled or correlated. They also illustrated several schemes for establishing the necessary reference state and demonstrated the accuracy of each. While, for homogeneous media, full-spectrum k-distribution (FSK) methods achieve LBL accuracy at a tiny fraction of LBL's computational cost, significant errors may occur when dealing with inhomogeneous media, because neither the scaled nor the correlated assumptions are ever truly accurate. The resulting errors have been discussed by Modest [6], as has the applicability of either model.

In addition to these drawbacks of the FSK methods, several limitations exist and are addressed in the present paper. The three major limitations are (1) difficulty of assembling accurate full-spectrum k-distributions for multi-component gas mixtures from full-spectrum k-distributions for the individual gas components, (2) inability to add nongray scattering particles to a precalculated full-spectrum k-distribution, and (3) inability of the method to accommodate nongray scattering particles and/or nongray wall reflectances. These limitations may all be conquered by constructing full- or part-spectrum k-distributions from narrow-band k-distributions for the individual gas component species.

2. Theoretical analysis

To fully understand the new adaptations of the FSK methods, it is essential to know how the FSK models are developed. The k-distribution serves to reorder the erratic spectral absorption coefficient of participating gaseous media into a monotonically increasing function over a narrow band, part or full spectrum in order to decrease the number of radiative transfer equation (RTE) evaluations necessary to solve a particular problem. For this reason, a brief review of the development of the RTE for the various k-distributions is given below followed by the information required to implement the new models.

2.1. Narrow-band RTE

The spectral RTE for an absorbing/emitting and scattering medium is expressed as [7]

$$\frac{\mathrm{d}I_\eta}{\mathrm{d}s} = \kappa_\eta(\underline{\phi},\eta)\left(I_{\mathrm{b}\eta}(T) - I_\eta\right) - \sigma_{\mathrm{s}\eta}(\underline{\phi}_s,\eta)\left(I_\eta - \frac{1}{4\pi}\int_{4\pi} I_\eta(\hat{s}')\Phi_\eta(\underline{\phi}_s,\hat{s},\hat{s}',\eta)\,\mathrm{d}\Omega'\right), \tag{1}$$

where $I_{\mathrm{b}\eta}$ is the Planck function, κ_η the absorption coefficient, $\sigma_{\mathrm{s}\eta}$ the scattering coefficient, Φ_η the scattering phase function; $\underline{\phi}$ and $\underline{\phi}_s$ are arrays of state variables that affect each's value [i.e.,

$\underline{\phi}=(T, p, \underline{x})$ contains the properties of the gas with $\underline{x}$ being the mole fraction vector, and $\underline{\phi}_s$ is a vector containing information of local particle properties, such as the number of particles per unit volume, N_t, and the particle radius, a]. Eq. (1) is first multiplied by Dirac's delta function, $\delta(k-\kappa_\eta(\underline{\phi}_0,\eta))$, where $\kappa_\eta(\underline{\phi}_0,\eta)$ is the medium's spectral absorption coefficient evaluated at a reference state $\underline{\phi}_0$, and k is an absorption coefficient variable. The RTE is then integrated over, and divided by, a small spectral interval, $\Delta\eta$, with $\Delta\eta$ small enough that Planck function, scattering coefficient, and scattering phase function are all essentially constant. This process serves to reorder the absorption coefficient in the equation and yields

$$\frac{\mathrm{d}I_k}{\mathrm{d}s}=k^*(\underline{\phi},k)\left(f(\underline{\phi}_0,k)I_{\mathrm{b}\eta}(T)-I_k\right)-\sigma_{\mathrm{s}\eta}(\underline{\phi}_s,\eta)\left(I_k-\frac{1}{4\pi}\int_{4\pi}I_k(\hat{s}')\Phi_\eta(\underline{\phi}_s,\hat{s},\hat{s}',\eta)\,\mathrm{d}\Omega'\right), \quad (2)$$

provided that every wavenumber wherever $\kappa_\eta(\underline{\phi}_0,\eta)$ has one and the same value k, $\kappa_\eta(\underline{\phi},\eta)$ always also has one unique value $k^*(\underline{\phi},k)$, (i.e., the absorption coefficient is *correlated* [6]). With the RTE reordered in terms of the absorption coefficient variable k, the spectral intensity I_η will be the same for each such occurrence described above and I_k can be defined as

$$I_k=\frac{1}{\Delta\eta}\int_{\Delta\eta}I_\eta(\eta)\delta\left(k-\kappa_\eta(\underline{\phi}_0,\eta)\right)\,\mathrm{d}\eta=I_\eta(k)f(\underline{\phi}_0,k), \quad (3)$$

in which $f(\underline{\phi}_0,k)$ is the k-distribution function for a narrow band at the reference state, defined as

$$f(\underline{\phi}_0,k)=\frac{1}{\Delta\eta}\int_{\Delta\eta}\delta\left(k-\kappa_\eta(\underline{\phi}_0,\eta)\right)\,\mathrm{d}\eta. \quad (4)$$

The k-distribution is a probability density function (PDF), giving the probability that the absorption coefficient will attain a value of k. The RTE is more conveniently solved by expressing it in terms of the cumulative k-distribution function at the reference state, or

$$g(\underline{\phi}_0,k)=\int_0^k f(\underline{\phi}_0,k)\,\mathrm{d}k, \quad (5)$$

leading to

$$\frac{\mathrm{d}I_g}{\mathrm{d}s}=k^*(\underline{\phi},g)\left(I_{\mathrm{b}\eta}(T)-I_g\right)-\sigma_{\mathrm{s}\eta}(\underline{\phi}_s,\eta)\left(I_g-\frac{1}{4\pi}\int_{4\pi}I_g(\hat{s}')\Phi_\eta(\underline{\phi}_s,\hat{s},\hat{s}',\eta)\,\mathrm{d}\Omega'\right), \quad (6)$$

where $I_g=I_k/f(\underline{\phi}_0,k)$, since $f(\underline{\phi}_0,k)$ is independent of location s. The average narrow band intensity can be determined after solving the RTE, using any arbitrary solution method, for the reordered spectral intensity, I_g, as

$$\bar{I}_\eta=\frac{1}{\Delta\eta}\int_{\Delta\eta}I_\eta\,\mathrm{d}\eta=\int_0^\infty I_k f(\underline{\phi}_0,k)\,\mathrm{d}k=\int_0^1 I_g\,\mathrm{d}g. \quad (7)$$

2.2. Full spectrum RTE

The development of the RTE for the full spectrum k-distribution method is similar to that for the narrow band except that integrations are now done over the entire spectrum instead of a small spectral interval. This leads to [6]

$$\frac{\mathrm{d}I_k}{\mathrm{d}s}=k^*(\underline{\phi},k)\left(f(T,\underline{\phi}_0,k)I_{\mathrm{b}}(T)-I_k\right)-\sigma_{\mathrm{s}}(\underline{\phi}_s)\left(I_k-\frac{1}{4\pi}\int_{4\pi}I_k(\hat{s}')\Phi(\underline{\phi}_s,\hat{s},\hat{s}')\,\mathrm{d}\Omega'\right), \quad (8)$$

provided again that every wavenumber across the entire spectrum where $\kappa_\eta(\underline{\phi}_0,\eta)=k$, we must, for a correlated absorption coefficient, also have a unique value for $\kappa_\eta(\underline{\phi},\eta)=k^*(\underline{\phi},k)$. Note that the scattering properties' dependence on wavenumber has been dropped in Eq. (8) since they must be gray for absorption coefficient reordering to hold. The full spectrum k-distribution and I_k are now expressed as

$$f(T,\underline{\phi}_0,k)=\frac{1}{I_\mathrm{b}}\int_0^\infty I_{\mathrm{b}\eta}(T)\delta\left(k-\kappa_\eta(\underline{\phi}_0,\eta)\right)\,\mathrm{d}\eta \tag{9}$$

and

$$I_k=\int_0^\infty I_\eta\delta\left(k-\kappa_\eta(\underline{\phi}_0,\eta)\right)\,\mathrm{d}\eta. \tag{10}$$

In terms of the cumulative k-distribution,

$$g(T,\underline{\phi}_0,k)=\int_0^k f(T,\underline{\phi}_0,k)\,\mathrm{d}k=\int_0^{k^*} f(T,\underline{\phi},k^*)\,\mathrm{d}k^*=g(T,\underline{\phi},k^*), \tag{11}$$

the RTE now becomes [6]:

$$\frac{\mathrm{d}I_g}{\mathrm{d}s}=k^*(T_0,\underline{\phi},g)\left(a(T,T_0,g)I_\mathrm{b}(T)-I_g\right)-\sigma_\mathrm{s}(\underline{\phi}_s)\left(I_g-\frac{1}{4\pi}\int_{4\pi}I_g(\hat{s}')\Phi(\underline{\phi}_s,\hat{s},\hat{s}')\,\mathrm{d}\Omega'\right), \tag{12}$$

where

$$I_g=I_k/f(T_0,\underline{\phi}_0,k), \tag{13}$$

$$a(T,T_0,g)=f(T,\underline{\phi}_0,k)/f(T_0,\underline{\phi}_0,k) \tag{14}$$

and $k^*(T_0,\underline{\phi},g)$ is the k vs. g distribution, as given by Eq. (11), with the absorption coefficient evaluated at the local conditions $\underline{\phi}$ and the Planck function at the reference temperature T_0 [6].

Similar to the narrow-band distribution, the reordered spectral intensity, I_g, can be obtained from the modified RTE, Eq. (12), and the spectrally integrated intensity is evaluated as [6]

$$I=\int_0^\infty I_\eta\,\mathrm{d}\eta=\int_0^\infty I_k f(T_0,\underline{\phi}_0,k)\,\mathrm{d}k=\int_0^1 I_g\,\mathrm{d}g. \tag{15}$$

The full-spectrum k-distributions given by Eqs. (9) and (11) can be calculated directly from spectral databases such as HITRAN [8] or HITEMP [9]. However, if a database of narrow-band k-distributions is available, full-spectrum distributions are much more efficiently assembled from their narrow-band cousins as

$$\begin{aligned}
f(T,\underline{\phi}_0,k)&=\frac{1}{I_\mathrm{b}(T)}\int_0^\infty I_{\mathrm{b}\eta}(T)\delta\left(k-\kappa_\eta(\underline{\phi}_0,\eta)\right)\,\mathrm{d}\eta\\
&=\frac{1}{I_\mathrm{b}}\sum_{j\in[\text{all NBs}]}\int_{\Delta\eta_j}I_{\mathrm{b}\eta}\delta\left(k-\kappa_\eta(\underline{\phi}_0,\eta)\right)\,\mathrm{d}\eta\\
&\cong\sum_{j\in[\text{all NBs}]}\frac{I_{\mathrm{b}j}}{I_\mathrm{b}}\frac{1}{\Delta\eta_j}\int_{\Delta\eta_j}\delta\left(k-\kappa_\eta(\underline{\phi}_0,\eta)\right)\,\mathrm{d}\eta\\
&=\sum_{j\in[\text{all NBs}]}\frac{I_{\mathrm{b}j}}{I_\mathrm{b}}f_j(\underline{\phi}_0,k),
\end{aligned} \tag{16}$$

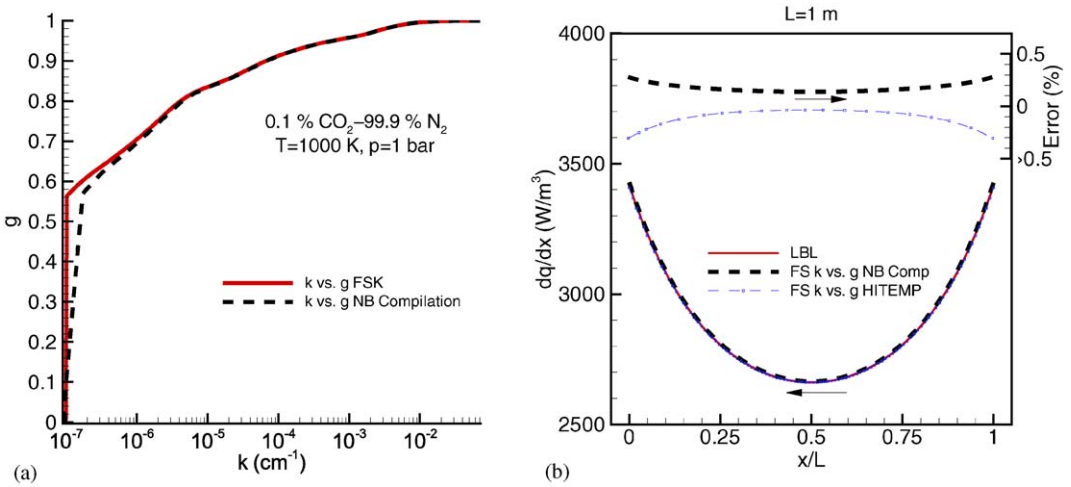

Fig. 1. Assembly of full-spectrum k-distributions from a narrow-band database: (a) k vs. g distributions, and (b) divergence of heat flux in a homogeneous slab.

where

$$I_{bj} = \int_{\Delta\eta_j} I_{b\eta}(T)\,d\eta \tag{17}$$

is the Planck function integrated over narrow band $\Delta\eta_j$. Equivalently, since the Planck function is nearly constant over the narrow band [i.e., $I_{b\eta}(T,\eta) \cong I_{b\eta}(T)_{\eta\in[\Delta\eta_j]}$], I_{bj} can also be expressed by $I_{b\eta}$ evaluated at the center of narrow band j multiplied by $\Delta\eta_j$, the narrow band's width. The cumulative k-distribution can also be assembled similarly as

$$g(T,\underline{\phi}_0,k) = \sum_{j\in[\text{all NBs}]} \frac{I_{bj}}{I_b}\, g_j(\underline{\phi}_0,k). \tag{18}$$

To illustrate the results of such a compilation, an example is given in Fig. 1a, showing the k-distributions for a N_2–CO_2 mixture at 1000 K and a total pressure of 1 bar containing a small amount (0.1%) of CO_2. The solid line was generated from LBL data and the dashed line compiled from precalculated and databased narrow-band distributions described in the following section. Discrepancies are apparent at low k-values, which are attributed to the fact that our compact narrow-band database uses very few points to resolve small k's. Other discrepancies may arise from numerical precision errors and the fact that the Planck function may not necessarily be constant over all narrow bands in a particular problem. Fig. 1b is a plot of the gradient of the radiative heat flux for a one-dimensional, homogeneous, 1 m thick slab, for the same gas mixture previously described, bounded by cold, black walls. This problem was solved on a LBL basis, a full-spectrum k-distribution basis calculated directly from HITEMP and also on a FSK basis with the full-spectrum k-distribution assembled from our narrow-band database. The P-1 approximation [7] was used as the RTE solver for both the LBL and k-distribution methods. Since, for this problem, the medium is homogeneous, the full-spectrum k-distribution method is "exact," i.e., the only inaccuracy arises from the fineness of the resolution with which the k-distribution is assembled. The same is true for the narrow-band

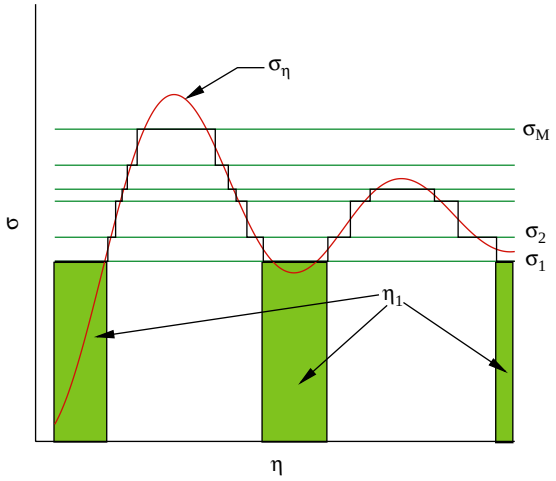

Fig. 2. Spectral grouping of nongray scattering coefficient.

k-distribution (here using a much coarser resolution) except that these may also incur small errors due to the assumption of a constant Planck function across each narrow band. The figure shows that the errors in the full-spectrum k-distribution that was generated from the narrow-band k-distributions have essentially no effect on the prediction of heat transfer. This is because most of the inaccuracies are at small k-values, which are relatively unimportant unless the optical thickness of the problem is extremely large. It is also worthwhile to note, although not shown here, that solving the problem over each narrow-band individually and summing the contributions of each yielded the same result within machine precision, as compiling the narrow bands into a single full-spectrum k-distribution before solving. For all subsequent examples, LBL will continue to be the benchmark, the assumption of a correlated absorption coefficient will be used and the P-1 approximation will be employed as the RTE solver.

2.3. Part-spectrum RTE

It is impossible to account for various nongray background properties, such as scattering coefficient, scattering phase function, wall reflectance, etc., with the full-spectrum k-distribution model. However, by grouping together spectral regions with similar background properties into M part-spectrum distributions, greater accuracy can be achieved than by assuming gray properties for a full-spectrum distribution, albeit at an M-fold computational cost. An example of how such part spectrum-grouping may be done to deal with a problem involving a nongray scattering coefficient is illustrated in Fig. 2 (for $M = 6$ different spectral values).

2.3.1. Part-spectrum RTE development

To develop the RTE for a part-spectrum distribution, the same procedure is followed as for the full spectrum, except that the integration is now done only over the spectral regions of interest.

The RTE for such a part-spectrum is then expressed as [10]

$$\frac{\mathrm{d}I_{gm}}{\mathrm{d}s} = k^*(T_0, \underline{\phi}, g_m)\left(a_m(T, T_0, g_m) I_\mathrm{b}(T) - I_{gm}\right) - \sigma_{sm}(\underline{\phi}_s) \times \left(I_{gm} - \frac{1}{4\pi}\int_{4\pi} I_{gm}(\hat{s}')\Phi_m(\underline{\phi}_s, \hat{s}, \hat{s}')\,\mathrm{d}\Omega'\right), \quad m = 1, M, \tag{19}$$

where m is an index identifying each part spectrum. The part-spectrum k-distribution is then defined as

$$f_m(T, \underline{\phi}_0, k) = \frac{1}{I_\mathrm{b}(T)}\int_{\eta\in[\eta_m]} I_{\mathrm{b}\eta}(T)\delta\left(k_m - \kappa(\underline{\phi}_0, \eta)\right)\,\mathrm{d}\eta, \tag{20}$$

$$I_{gm} = \frac{\int_{\eta\in[\eta_m]} I_\eta \delta\left(k - \kappa(\underline{\phi}_0, \eta)\right)\mathrm{d}\eta}{f_m(T_0, \underline{\phi}_0, k)}, \tag{21}$$

$$a_m(T, T_0, g_m) = f_m(T, \underline{\phi}_0, k)/f_m(T_0, \underline{\phi}_0, k). \tag{22}$$

The range of each g_m is limited by the fact that it represents only a part of the whole spectrum. Ordering of the part-spectrum distributions and assignment of minimum values is arbitrary; the chosen structure given by Eq. (23) is one of many possible and was taken for convenience:

$$g_{m,\min} = \begin{cases} 0, & m = 1, \\ g_{m-1,\min} + \displaystyle\int_0^\infty f_m\,\mathrm{d}k = g_{m-1,\max}, & 2 < m < M, \end{cases} \tag{23a}$$

$$g_m(T_0, \underline{\phi}_0, k) = g_{m,\min} + \int_0^k f_m(T_0, \underline{\phi}_0, k)\,\mathrm{d}k. \tag{23b}$$

As with narrow-band and full-spectrum k-distributions, the reordered spectral intensity can be calculated from the modified RTE, Eq. (19), and used to evaluate the part-spectrum integrated intensity as

$$I_m = \int_{\eta\in[\eta_m]} I_\eta\,\mathrm{d}\eta = \int_0^\infty I_{km} f_m(T_0, \underline{\phi}_0, k)\,\mathrm{d}k = \int_{g_{m,\min}}^{g_{m,\max}} I_{gm}\,\mathrm{d}g_m, \quad m = 1, M. \tag{24}$$

From this, the intensity integrated over the full spectrum can be recovered as

$$I = \int_0^\infty I_\eta\,\mathrm{d}\eta = \sum_{m=1}^{M} I_m. \tag{25}$$

2.3.2. Part-spectrum k-distributions from narrow band k-distributions

Part-spectrum cumulative k-distributions can be generated from their definition in Eq. (20) using a high-resolution database but they can also be generated from narrow-band k-distribution data as

$$f_m(T, \underline{\phi}, k) = \frac{1}{I_\mathrm{b}(T)}\sum_{\Delta\eta_j\in[\eta_m]}\int_{\Delta\eta_j} I_{\mathrm{b}\eta}(T)\delta\left(k - \kappa_\eta(\underline{\phi}, \eta)\right)\mathrm{d}\eta \tag{26}$$

and, since $I_{b\eta}$ is relatively constant over each narrow band, multiplying and dividing by $\Delta\eta_j$ and the use of Eq. (3) gives

$$f_m(T,\underline{\phi},k) \cong \sum_{\Delta\eta_j\in[\eta_m]} \frac{I_{bj}}{I_b}\frac{1}{\Delta\eta_j}\int_{\Delta\eta_j}\delta\big(k-\kappa_\eta(\underline{\phi},\eta)\big)\,d\eta = \sum_{j\in[\eta_m]}\frac{I_{bj}}{I_b}f_j(\underline{\phi},k), \tag{27}$$

where

$$I_{bj}(T) = \int_{\Delta\eta_j} I_{b\eta}(T)\,d\eta. \tag{28}$$

Using Eq. (23) leads to

$$g_m(T,\underline{\phi},k) = g_{m,\min} + \int_0^k \sum_{\Delta\eta_j\in[\eta_m]}\frac{I_{bj}}{I_b}f_j(\underline{\phi},k)\,dk = g_{m,\min} + \sum_{\Delta\eta_j\in[\eta_m]}\frac{I_{bj}}{I_b}g_j(\underline{\phi},k), \tag{29}$$

where $g_j(\underline{\phi},k)$ represents a narrow-band cumulative k-distribution for a gas at state $\underline{\phi}$.

3. Narrow band cumulative *k*-distribution database

In order to assemble full- or part-spectrum k-distributions for gas and particle mixtures, an accurate narrow band database must first be generated. For the present study, the database generation was limited to CO_2 and H_2O. The spectral data used in their generation were taken from the HITEMP database [9].

First, the global maximum and minimum pressure-based absorption coefficients were determined, over every narrow band, gas state, and gas specie. With these, a fixed set of k-bins were arranged in a power distribution given by

$$\Delta(k^q) = [(k_{\max})^q - (k_{\min})^q]/(N_k - 1), \tag{30}$$

$$k_i^q = k_{\min}^q + (i-1)\Delta(k^q), \quad i = 1,\ N_k, \tag{31}$$

where $k_{\min}$ is the global minimum κ_η-value for any state, $k_{\max}$ is the global maximum κ_η-value, N_k is the total number of k values between $k_{\min}$ and $k_{\max}$, which are considered for the construction of all k-distributions and q is an exponential factor used to generate a skewed distribution that places more points at smaller k-values than a linear distribution, but fewer than a logarithmic distribution. In our work $q = 0.05$ was used, which gives values spanning several orders of magnitude but puts more emphasis on larger values (which tend to be of most importance for heat transfer applications) and $N_k = 5000$.

The spectral data from HITEMP were generated at 0.01 cm^{-1} resolution for 242 narrow bands at 23 temperatures and five mole fractions for H_2O and three for CO_2. More mole fraction intervals were used for H_2O because of its line broadening characteristics that are more strongly dependent upon concentration. The temperatures considered were between 300 and 2500 K, and the mole fractions were equally spaced between 0.0 and 1.0. The widths of the narrow bands were distributed as given in Table 1. The band widths were arranged as stated for reasons of Planck function variation and narrow band importance. Narrow-band k-distributions for gas states not contained in the database were generated by simple linear interpolation in mole fraction and temperature. More elaborate interpolation schemes were found unnecessary in all cases tested.

Table 1
Nominal narrow band ranges for k-distribution database

Spectral range	Narrow-band width	Narrow-band number
200–4000 cm^{-1}	$\Delta\eta = 25\ cm^{-1}$	1–152
4000–5000 cm^{-1}	$\Delta\eta = 50\ cm^{-1}$	153–172
5000–10,000 cm^{-1}	$\Delta\eta = 100\ cm^{-1}$	173–222
10,000–15,000 cm^{-1}	$\Delta\eta = 250\ cm^{-1}$	223–252

Since many k-distributions exhibit a rapid increase in g over a very narrow k-range, the interpolation in mole fraction and temperature is most effectively carried out at fixed g-values. Because the distributions are first assembled at fixed k-values, it was advantageous to fit and store the data in a format that utilizes fixed g-values. This new format utilizes a distribution of fixed g-values from a Gaussian distribution that varies from 0 to 1. These new g-values are the same for all narrow bands, gas states, and gas species. The number of data points for each narrow band could by choice be variable, depending on the narrow band's importance, but was set to a constant and relatively small value of 100 here. The k-values for these Gaussian g-points were fit from the calculated k-distributions using a monotonic spline function. A more accurate and refined form of this database is currently under development [11].

4. k-Distributions for gas mixtures

In the case of a multi-specie gas mixture, the k-distributions of each component specie will have to be combined into a single k-distribution. However, exact mixing of k-distributions is impossible because the k-distributions never retain any information pertaining to the spectral location of the individual absorption lines.

Taine and Soufiani [12] have shown that multiplying the transmissivities of I individual gas species together to obtain a mixture transmissivity can be very accurate when compared to direct LBL transmissivity calculations for the mixture, i.e.,

$$\tau_{\mathrm{mix}} \cong \prod_{i=1}^{I} \tau_i. \tag{32}$$

This holds true as long as the absorption coefficients of the different gas species in the mixture are statistically uncorrelated. Fig. 3 demonstrates such a test case for the transmissivity of a 100 cm thick, 50% CO_2–50% H_2O mixture at 1200 K and 1 bar over the 2.7 μm range at a resolution of 25 cm^{-1}. The difference between the actual transmissivity and the transmissivity attained through multiplication is essentially negligible, never exceeding 0.004. However, Taine and Soufiani did not attempt to produce a mixture k-distribution from individual component specie k-distributions based on this observation.

Several approximate mixing models for k-distributions have been proposed that rely on assumptions about the statistical relationships between the absorption lines of the individual species, mostly by Solovjov and Webb [13], such as their convolution, superposition, multiplication and hybrid approaches. All of these approaches produce a single mixture k-distribution, but rely on different assumptions and methodologies to achieve their goal.

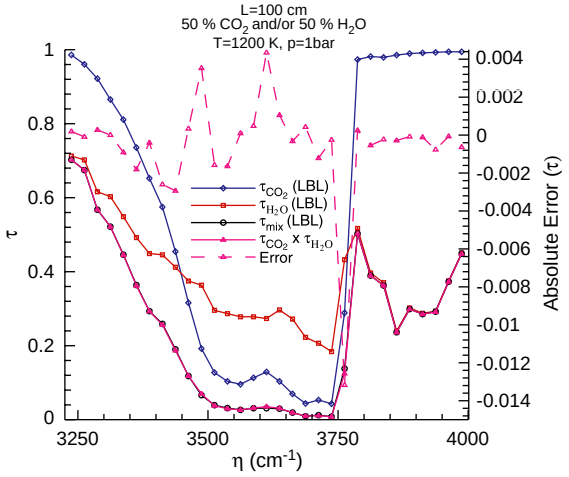

Fig. 3. Narrow-band transmissivity of CO_2–H_2O mixture from LBL calculations.

The convolution scheme uses a sort of convolution integral of the component k-distributions. According to Solovjov and Webb, this model relies on the assumption of uncorrelated absorption coefficients between component gas species. The superposition approach relies on the assumption that the spectral lines of the component specie do not significantly overlap, leading to additive g-values for the mixture, or

$$g(k) = \left(\sum_{i=1}^{I} g_i(k) \right) - (I - 1), \tag{33}$$

where $g(k)$ is the mixture k-distribution and $g_i(k)$ are the k-distributions for the component species. The multiplication scheme calculates mixture g-values from

$$g(k) = \prod_{l} g_l(k). \tag{34}$$

According to Solovjov and Webb, this model also relies on the assumption of uncorrelated absorption coefficients between component gas species through the multiplication property of the probability of independent events. Although this model generally provides good results, the statistical validity of multiplying cumulative distribution functions appears questionable. This is corroborated by Fig. 4, which shows the transmissivity calculated from k-distributions mixed by multiplication and the transmissivity calculated from LBL data for the same gas slab as depicted in Fig. 3. Solovjov and Webb noted that the multiplication model is valid for small k-values, while the superposition model performs best for large k-values. For this reason they developed the hybrid model, which makes use of the k-distributions developed with both, the multiplication and superposition, models by combining them using logarithmic weighting.

Mixing of full-spectrum k-distributions with these models or others, using a narrow-band database, may be carried out in one of two ways. In the first the mixing is done on a narrow band basis followed by combination into full- or part-spectrum distributions. In the other the full- or part-spectrum distribution for all component species are assembled first followed by mixing.

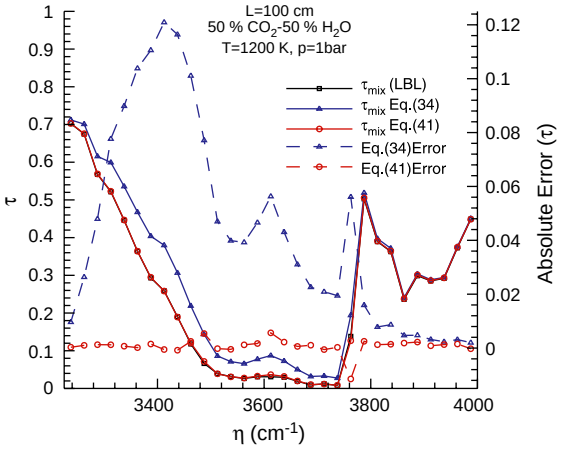

Fig. 4. Narrow-band transmissivity of CO_2–H_2O mixture from k-distributions.

4.1. New narrow-band mixing model

Through simple mathematical manipulation, it is possible to extend the idea of uncorrelated absorption coefficients, resulting in the transmissivity given by Eq. (32) to mixing of cumulative k-distributions. We begin by noting that the definition of the transmissivity, in terms of the k-distribution for a single absorbing specie,

$$\tau_i = \int_0^\infty \mathrm{e}^{-k_i L} f_i(k)\,\mathrm{d}k_i, \tag{35}$$

is also the definition of the Laplace transform of $f_i(k)$ [14]. Using this and the product of transmissivities model, the transmissivity of a mixture may be expressed as the product of the Laplace transforms of the component k-distributions, or

$$\tau_{\mathrm{mix}} = \mathscr{L}[f_{\mathrm{mix}}(k)] = \prod_{i=1}^{I} \mathscr{L}[f_i(k)]. \tag{36}$$

In terms of the cumulative k-distributions, the transmissivity of an individual component is given by

$$\tau_i = \int_0^1 \mathrm{e}^{-k_i L}\,\mathrm{d}g_i \tag{37}$$

and for a binary mixture this becomes

$$\tau_{\mathrm{mix}} = \mathscr{L}[f_{\mathrm{mix}}(k)] = \int_0^1 \mathrm{e}^{-k_1 L}\,\mathrm{d}g_1 \int_0^1 \mathrm{e}^{-k_2 L}\,\mathrm{d}g_2 = \int_{g_1=0}^1 \int_{g_2=0}^1 \mathrm{e}^{-[k_1(g_1)+k_2(g_2)]L}\,\mathrm{d}g_2\,\mathrm{d}g_1. \tag{38}$$

Using the integral property of the Laplace transform we obtain

$$\mathscr{L}\left[\int_0^k f_{\mathrm{mix}}(k)\right] = \mathscr{L}[g_{\mathrm{mix}}(k)] = \left(\int_{g_1=0}^1 \int_{g_2=0}^1 \mathrm{e}^{-[k_1(g_1)+k_2(g_2)]L}\,\mathrm{d}g_2\,\mathrm{d}g_1\right)\frac{1}{L},$$

$$= \int_{g_1=0}^1 \int_{g_2=0}^1 \frac{\mathrm{e}^{-[k_1(g_1)+k_2(g_2)]L}}{L}\,\mathrm{d}g_2\,\mathrm{d}g_1 \tag{39}$$

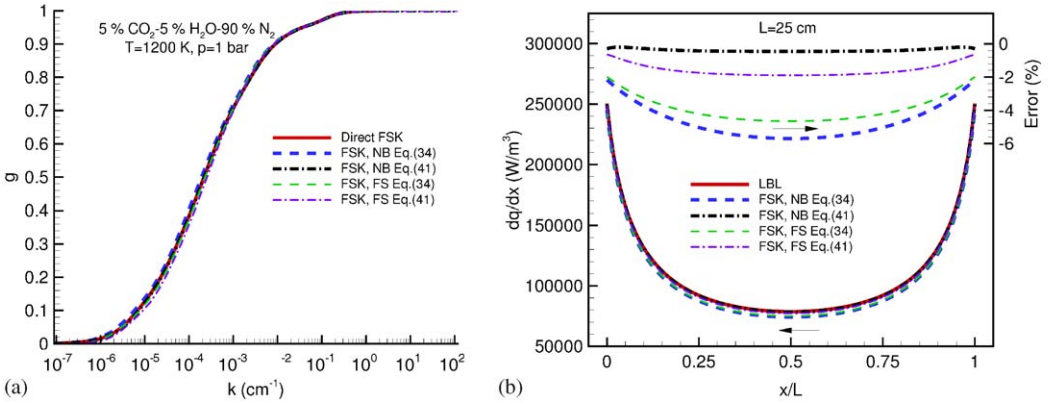

Fig. 5. Full spectrum mixing: (a) k vs. g distributions for CO_2–H_2O mixtures and (b) divergence of heat flux inside homogeneous slab.

or when the inverse transform is taken, with H being the Heaviside step function,

$$g_{\mathrm{mix}}(k_{\mathrm{mix}}) = \int_{g_1=0}^{1} \int_{g_2=0}^{1} H[k_{\mathrm{mix}} - (k_1 + k_2)]\, \mathrm{d}g_2\, \mathrm{d}g_1 = \int_{g_1=0}^{1} g_2(K_{\mathrm{mix}} - k_1)\, \mathrm{d}g_1 \tag{40}$$

In the second, once integrated expression, it is assumed that $g_i(k < k_{i,min}) = 0$ (i.e., all absorption coefficients are above $k_{i,min}$) and $g_i(k < k_{i,max}) = 1$ (i.e., all absorption coefficients are below $k_{i,max}$). This relation may also be readily extended to mixtures of I species,

$$g_{\mathrm{mix}}(k_{\mathrm{mix}}) = \int_{g_1=0}^{1} \cdots \int_{g_I=0}^{1} H[k_{\mathrm{mix}} - (k_1 + \cdots + k_I)]\, \mathrm{d}g_I \cdots \mathrm{d}g_1. \tag{41}$$

This integral may be evaluated by multiple Gaussian quadrature, leading to a single mixture k-distribution at specific k-values while using the component k-distributions stored at quadrature points with their associated weights. The k-values for this new mixture distribution must be predetermined and chosen such that they cover the entire range of values of all component species. Carrying out mixing on either a narrow-band or full-spectrum basis with this new model has consistently outperformed the multiplication model on either basis as well. This is demonstrated in Fig. 4 which shows significantly larger error for multiplicative mixing as opposed to the new scheme given by Eq. (41). The accuracy of mixing models for full-spectrum k-distributions is shown in Fig. 5, in which a 90% N_2–5% CO_2–5% H_2O mixture at 1200 K and 1 bar is examined. The chosen concentration values are not contained in our narrow-band database, thus providing a check for our linear interpolation scheme. In Fig. 5a, the cumulative k-distribution calculated directly from the mixture absorption coefficient is compared with the distributions generated by multiplicative mixing and the new mixing model (carrying out the mixing on a narrow-band and full-spectrum basis in both cases). While difficult to distinguish in the figure, the new mixing model carried out on a narrow-band basis outperforms its full-spectrum brother and is substantially more accurate than the multiplication scheme carried out on either basis, especially for g-values less than 0.9. In Fig. 5b, the divergence of the heat flux is shown as given inside a one-dimensional 25 cm thick slab with the gas at the previously described state, bounded by cold, black walls. Because the slab is homogenous, the FSK method is "exact" and all errors arise

from the mixing of the k-distributions (aside from the inaccuracies in the individual component gas specie k-distributions). The figure illustrates that the new mixing model is a vast improvement over the multiplicative scheme with respect to the accuracy of heat transfer calculations.

5. Nongray absorbing particles

When dealing with practical problems, one often encounters absorbing particles such as soot in the medium. Within a narrow band, the absorption coefficient of a particle cloud is usually relatively constant and, thus, the absorption of particles can be simply treated as a DC addition to the narrow band cumulative k-distribution. This is achieved by determining the average particle absorption coefficient across the narrow band and then adding it to the k-distribution of that narrow band. In the presence of a gas mixture, the narrow-band mixing should be carried out before particle absorption is added. This serves to not interfere with the statistical uncorrelatedness of the individual gas specie absorption coefficients.

To demonstrate the effectiveness of this type of treatment of absorbing particles, a calculation was performed on a homogeneous, 20 cm thick, one-dimensional slab bounded by cold, black walls consisting of a N_2–CO_2 mixture with 10% CO_2 at 1200 K and 1 bar and containing nongray soot with a volume fraction of $f_v = 10^{-7}$. The soot's complex index of refraction, $m = n - ik$, was modeled using the correlations developed by Chang and Charalampopoulos [15],

$$n = 1.811 + 0.1263 \ln\lambda + 0.0270 \ln^2\lambda + 0.0417 \ln^3\lambda, \tag{42}$$

$$k = 0.5821 + 0.1213 \ln\lambda + 0.2309 \ln^2\lambda - 0.0100 \ln^3\lambda, \tag{43}$$

where λ is the wavelength in μm. These correlations are valid over the wavelength range $0.4\ \mu m \leqslant \lambda \leqslant 30\ \mu m$. The soot's absorption coefficient was determined using the small particle limit of Rayleigh scattering for a cloud of non-uniform particles sizes [7] given by

$$\kappa_\lambda = \frac{36\pi nk}{(n^2 - k^2 + 2)^2 + 4n^2k^2} \frac{f_v}{\lambda}. \tag{44}$$

Full-spectrum k-distributions for this test case obtained directly from HITEMP, as well as from our narrow-band database with soot added as described in this section are shown in Fig. 6a, while the corresponding radiation sources are given in Fig. 6b. There is almost no distinguishable difference in the k-distributions and no substantial error in the heat transfer calculation, thus confirming the accuracy of this model.

6. Nongray scattering model

As indicated earlier, the part spectrum grouping method can be employed to treat nongray scattering (and/or nongray wall reflectances, etc.). This method uses M different spectral values for the scattering coefficient to approximate the scattering properties across the entire spectrum as indicated in Fig. 2. Each of these part-spectrum scattering coefficients may vary spatially according to

$$\sigma_{s\eta}(\underline{\phi}_s, \eta) \cong \sigma_m(\underline{\phi}_s)_{\eta \in [\eta_m]} \tag{45}$$

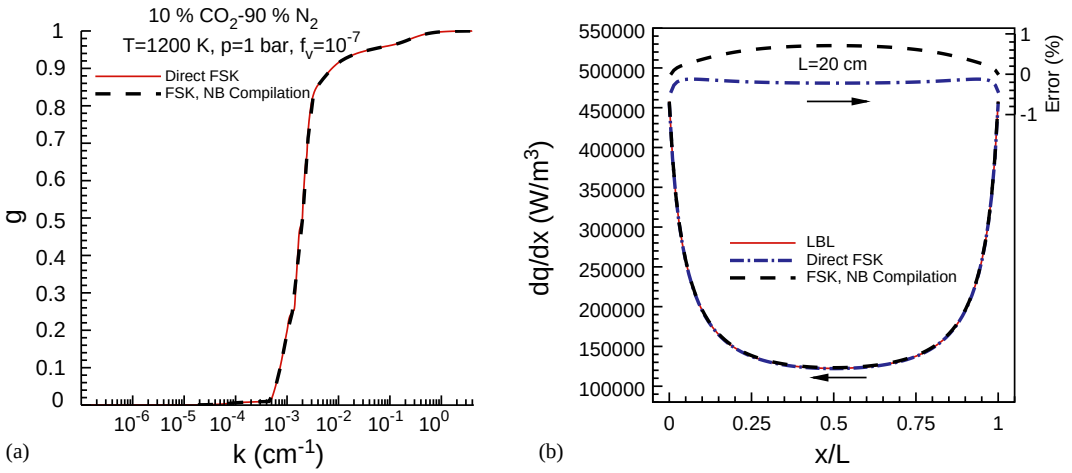

Fig. 6. Gas mixtures with nongray soot: (a) full-spectrum k vs. g distributions and (b) divergence of heat flux inside homogeneous slab.

and wall emittance according to

$$\varepsilon_\eta(\underline{r}_\mathrm{w},\eta) \cong \varepsilon_m(\underline{r}_\mathrm{w})_{\eta\in[\eta_m]}, \tag{46}$$

where $\underline{r}_\mathrm{w}$ is a vector pointing to a location on a wall, or both may obey these relations if both are nongray. For the present illustration, scattering will be assumed isotropic and wall reflectances gray, but other problems may be treated in an identical fashion. The narrow-band distributions will be combined into M different part spectra, each corresponding to a single gray scattering coefficient, $\sigma_m(\underline{\phi}_s)$.

6.1. Model development

In order to apply the part-spectrum k-distribution method, the scattering coefficient $\sigma_{s\eta}(\underline{\phi}_s,\eta)$ must be reformulated to obey Eq. (45). For the present illustration, we will only consider the simple case of a scaled scattering coefficient, i.e.,

$$\sigma_{s\eta}(\underline{\phi}_s,\eta) = \sigma_\eta(\eta)u_s(\underline{\phi}_s). \tag{47}$$

Such a scattering coefficient is found, for example, for particle clouds of larger particles ($2\pi a\eta \gg 1$, $ka > 1$, where $a =$ particle radius and $k =$ absorptive index of particle material), and particle clouds of uniform particle size.

First, the average scattering coefficient, $\bar{\sigma}_{\mathrm{nb},j}$, is evaluated for each narrow band as

$$\bar{\sigma}_{\mathrm{nb},j} = \frac{1}{\Delta\eta_j}\int_{\Delta\eta_j}\sigma_\eta\,\mathrm{d}\eta, \quad j = 1, J_\mathrm{nb}, \tag{48}$$

which is illustrated in Fig. 7. Note here that $\bar{\sigma}_{\mathrm{nb},j}$ is not a function of specific location because of the use of Eq. (47). Using the values of $\bar{\sigma}_{\mathrm{nb},j}$, the M nominal scattering values, σ_m are determined

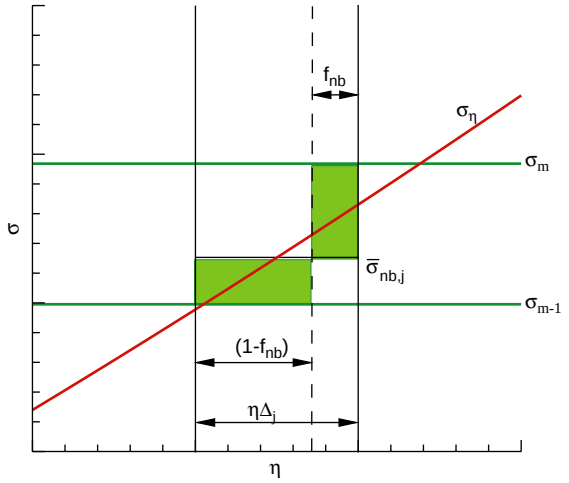

Fig. 7. Fractional narrow band grouping.

through optimization by minimizing the following function:

$$F = \sum_{j=1}^{J_{\mathrm{nb}}} (\bar{\sigma}_{\mathrm{nb},j} - \sigma_m)^2 w_j, \tag{49}$$

where σ_m is the nominal scattering value larger than and nearest to $\bar{\sigma}_{\mathrm{nb},j}$ and w_j is a weight function. In our calculations, w_j was set to the Planck function evaluated at the maximum system temperature and integrated over the narrow band $\Delta\eta_j$, i.e., weighting the narrow bands according to their contribution toward emission.

Once optimal nominal scattering values σ_m have been determined, M part-spectrum distributions are assembled by scanning over all narrow bands and assigning fractions of each narrow band to the two groups surrounding it, as determined by $\sigma_m > \bar{\sigma}_{\mathrm{nb},j} > \sigma_{m-1}$. The fraction of narrow band j

$$f_{\mathrm{nb},j} = \begin{cases} 0, & \bar{\sigma}_{\mathrm{nb},j} > \sigma_M, \\ \dfrac{\bar{\sigma}_{\mathrm{nb},j} - \sigma_{m-1}}{\sigma_m - \sigma_{m-1}}, & \sigma_M > \bar{\sigma}_{\mathrm{nb},j} > \sigma_1, \\ 1, & \bar{\sigma}_{\mathrm{nb},j} < \sigma_1 \end{cases} \tag{50}$$

is assigned to group m and the remainder of the band width, $1 - f_{\mathrm{nb},j}$, is assigned to group $m-1$, the lower bounding value as illustrated in Fig. 7. This allows the average narrow band scattering coefficient, $\bar{\sigma}_{\mathrm{nb},j}$, to be recovered exactly for all $\sigma_1 \leqslant \bar{\sigma}_{\mathrm{nb},j} \leqslant \sigma_M$. Values of $\bar{\sigma}_{\mathrm{nb},j}$ outside of these bounds are approximated by either σ_1 or σ_M. In addition to aiding in the recovery of $\bar{\sigma}_{\mathrm{nb},j}$, the fractions also represent the portion of each narrow band's wavenumber space to be included in the part spectrum k-distribution corresponding to each of the M scattering values. The cumulative k-distribution for this part spectrum is then

$$g_m(k) = \sum_{j=1}^{J_{\mathrm{nb}}} w_{j,m} \frac{I_{\mathrm{b}j}}{I_{\mathrm{b}}} g_j(k), \quad m = 1, M, \tag{51}$$

where

$$w_{j,m} = \begin{cases} 0, & \bar{\sigma}_{\mathrm{nb},j} < \sigma_{m-1}, \\ f_{\mathrm{nb},j}, & \sigma_{m-1} < \bar{\sigma}_{\mathrm{nb},j} < \sigma_m, \\ (1 - f_{\mathrm{nb},j}), & \sigma_m < \bar{\sigma}_{\mathrm{nb},j} < \sigma_{m+1}, \\ 0, & \bar{\sigma}_{\mathrm{nb},j} > \sigma_{m+1} \end{cases} \tag{52}$$

and $g_j(k)$ represents the narrow band cumulative k-distribution for a mixture of gases adjusted for particle absorption if present. Note that this scheme satisfies Eq. (23), i.e., the sum of all g_m-ranges adds to unity.

6.2. Sample calculations

To demonstrate the increased accuracy achieved with the part-spectrum model for nongray scattering, several test cases will be presented. These include a one-dimensional homogeneous slab, a one-dimensional slab with a homogeneous gas layer, but with scattering particles present across only half of the volume and finally, a two-dimensional inhomogeneous problem. For all of these test cases the same scattering behavior is assumed, defined by non-absorbing (dielectric) spheres with a radius of 10 μm and an index of refraction of $n = 1.3$. For the purpose of this illustration the scattering efficiency, Q_{sca}, is approximated by correlations for anomalous diffraction for a dielectric given by van de Hulst [7,16] as

$$Q_{\mathrm{ext}} = Q_{\mathrm{sca}} = 2 - \frac{4}{p}\left[\sin p - \frac{1 - \cos p}{p}\right], \tag{53}$$

where

$$p = 2x(n - 1) \tag{54}$$

and $x = 2\pi a/\lambda$ is the particle size parameter, and a the particle radius. This correlation is valid for near-dielectric spheres with an absorptive index $k \approx 0$ and with a refractive index close to 1, i.e., $|m - 1| \ll 1$ where $m = n - \mathrm{i}k$, the complex index of refraction. It is also valid for arbitrary values of $x|m - 1|$ provided that the particles are large, $x \gg 1$, as is the case in Fig. 8. Since we will assume isotropic scattering, the strongly forward-scattering peak due to diffraction is removed by subtracting $(1 - \mathrm{e}^{-0.1x})$ from Q_{sca} while not letting Q_{sca} fall below zero. The scattering coefficient, σ_{s}, then is approximated by

$$\sigma_\eta = Q_{\mathrm{sca}}\pi a^2 N_t = \pi a^2 N_t \left[2 - \frac{4}{p}\left(\sin p - \frac{1 - \cos p}{p}\right) - (1 - \mathrm{e}^{-0.1x})\right]. \tag{55}$$

While this leads to a somewhat artificial scattering coefficient, it provides—with its undulations as shown in Fig. 8—a severe test case for the part-spectrum k-distribution model (which will rarely occur in practical applications).

For the homogeneous, one-dimensional test case, N_t was taken as 1.25×10^{-12} m^{-3}. The gas is a 20 cm thick slab consisting of a 90% N_2–5% CO_2–5% H_2O mixture at 1050 K and 1 bar with a soot volume fraction of $f_{\mathrm{v}} = 10^{-6}$, and is bounded by cold, black walls. Again, values for concentration and temperature were chosen to force interpolation between the databased k-distributions, to capture

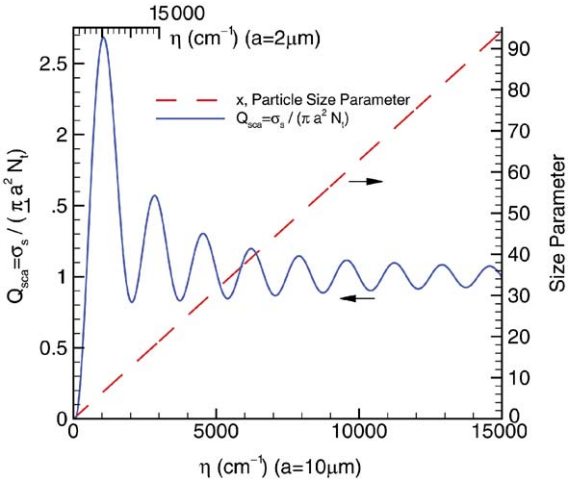

Fig. 8. Scattering parameters for sample calculations.

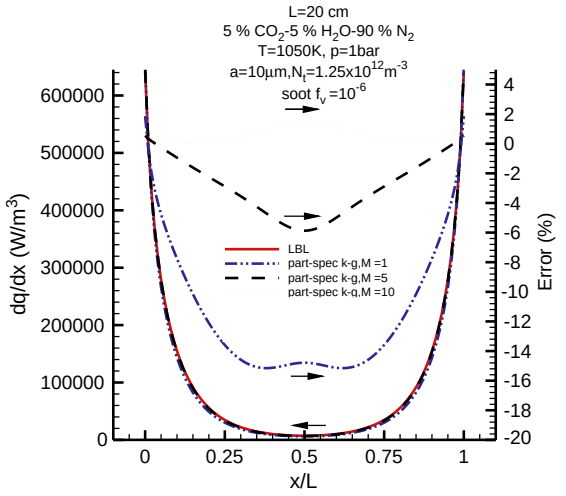

Fig. 9. Divergence of heat flux for a one-dimensional homogeneous gas state with a constant particle concentration.

errors caused by these interpolations. Fig. 9 shows the local divergence of the heat flux within the slab and illustrates the large improvement in accuracy by using five scattering groups when compared to a single gray value. It also illustrates the diminishing increase in accuracy achieved by going from five to 10 groups.

For the case with a step change in N_t, the problem considered is exactly the same as the homogeneous layer except that over the right half of the slab ($10\text{ cm} < x \leqslant 20\text{ cm}$) the medium is free of particles. The results, shown in Fig. 10, exhibit trends similar to that for the homogeneous case. More elaborate test cases with steps in temperature, gas concentration, and soot concentration were tested but did not produce significant errors when using a single scattering group (i.e., gray

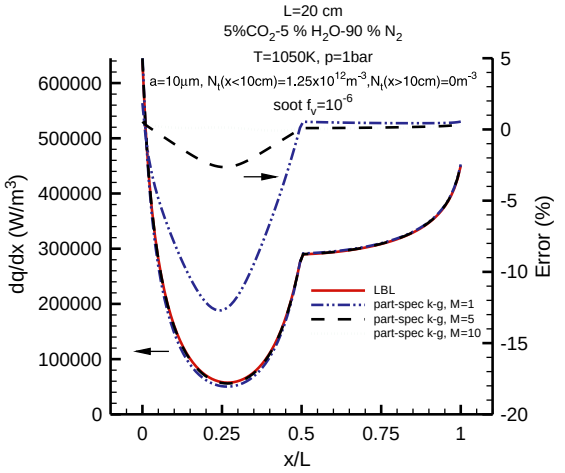

Fig. 10. Divergence of heat flux for a one-dimensional homogeneous gas state with a step in particle concentration.

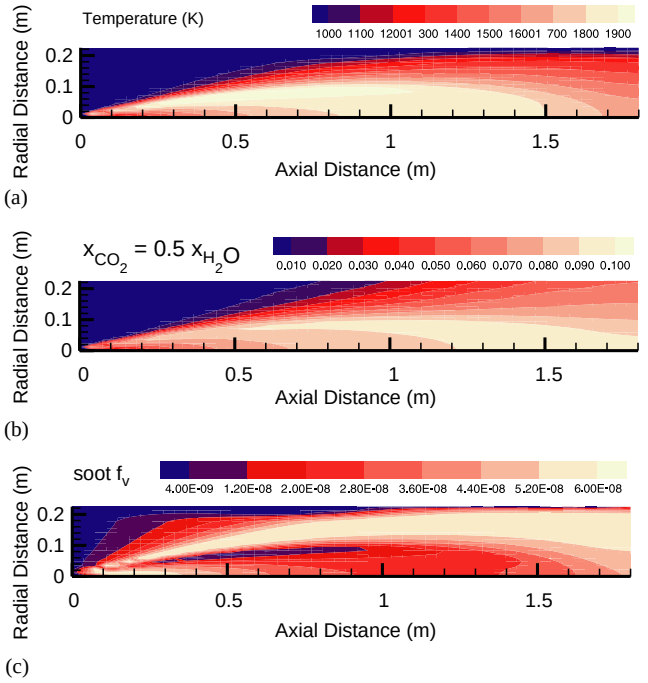

Fig. 11. Two-dimensional cylindrical methane combustor: (a) temperature and (b) concentration profiles.

scattering). This leads to the important conclusion that in many practical problems spectral variations of scattering properties do not strongly affect heat transfer results, thus allowing the more efficient use of full-spectrum methods and gray scattering.

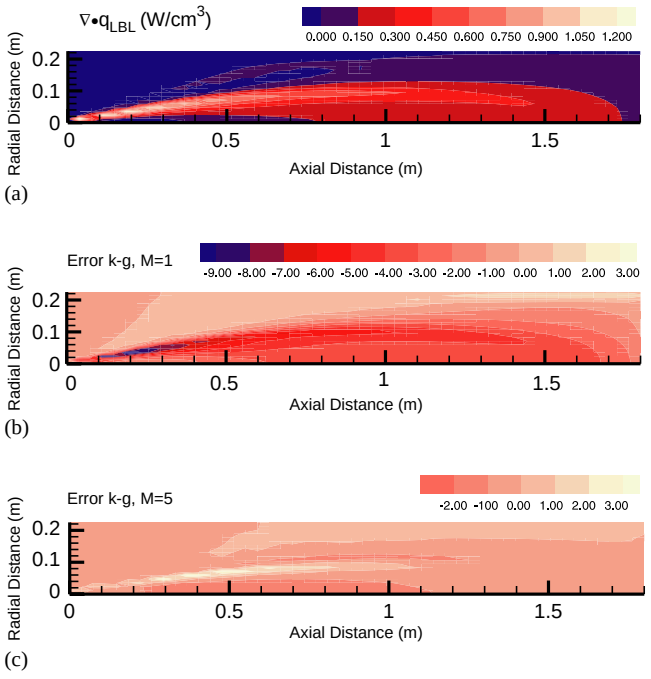

Fig. 12. Two-dimensional cylindrical methane combustor: (a) radiative heat source from LBL, (b) error using one scattering group (FSCK), and (c) error using five scattering groups (PSCK); error $= (\nabla \cdot q_{\mathrm{LBL}} - \nabla \cdot q_{k-g})/\nabla \cdot q_{k-g,\max}$.

For the two-dimensional sample problem, a simplified, cylindrical methane combustor is modeled. Radiation from methane in the system was neglected and the only participating gases considered are H_2O and CO_2. The temperature and concentration profiles are similar to those used by Zhang and Modest [10] and are shown in Figs. 11a and b, respectively. The enclosure walls are black and set to the temperature of the adjacent gas. Soot was included, with a temperature dependent volume fraction shown in Fig. 11c. This distribution is, of course, highly artificial, but it serves well to demonstrate the power and accuracy of the present method. The scattering parameters differ from the two previous sample problems, since using those properties resulted in only negligible errors in the two-dimensional case, even when scattering was approximated as gray ($M = 1$). The number of scattering particles per unit volume, $N_t = 7.62 \times 10^{12}\,\mathrm{m}^{-3}$, is assumed to be spatially constant across the entire domain except where the gas temperature is below 1050 K, where N_t is set to 0. In addition, the particle radius was reduced to $2\,\mu$m, thus maximizing nongrayness of the scattering coefficient (cf. Fig. 8, top abscissa). The divergence of the heat flux from LBL calculations (i.e., the radiative source term in the overall energy equation) is shown in Fig. 12a and the errors associated with one and five group models are depicted in Fig. 12b and c, respectively. Since the radiative source can be locally positive (emission outweighs absorption; hot regions) or negative (absorption exceeds emission; cold regions near inlet with mostly air and along centerline with mostly fuel) the relative error is defined in comparison with the maximum (positive) source within the combustor. The figures show that the maximum error occurs in the hottest regions for both the one and five group models (10% maximum error for gray scattering, $M = 1$, error using

$M=5$). This demonstrates the significant increase in accuracy attained by adopting a five group model over the gray one group model, whenever non-gray scattering has a noticeable impact. The case of $M = 20$ was also considered with little further improvement in accuracy (not shown), indicating that the remaining inaccuracies are due the approximation made by the k-distribution approach in nonhomogeneous media. Another, similar two-dimensional test case (not shown here) was used to confirm the accuracy of our narrow-band database and also our new mixing model. This problem was exactly the same as the previous one but neglects soot and scattering particles. In this case the relative error over the domain never exceeds 1%, thus quantifying the accuracy of our database, mixing model, and the FSCK approach in general.

7. Conclusion

A new set of methods have been developed to overcome several of the limitations of the FSK methods, based on efficient, on-the-fly compilation of full- and part-spectrum k-distributions from a narrow-band k-distribution database. A new narrow-band mixing model was introduced that, based on the assumption of uncorrelatedness between species, accurately recovers narrow band transmissivities of gas mixtures and allows the accurate assembly of mixture narrow-band and full-spectrum k-distributions from the single-specie narrow-band database. Secondly, it was shown how full-spectrum k-distributions for gas mixtures containing nongray absorbing particles (such as soot) can be assembled in an exact fashion from the same single-specie narrow-band database. Finally, a part-spectrum k-distribution model was developed to allow the accurate treatment of other nongray background properties (scattering, wall reflection) at a reasonable increase in computational cost. It was found that generally very few part spectra are needed to achieve accurate results and that, indeed, the assumption of gray scattering tends to give reasonable accuracy (thus allowing the use of the most efficient full-spectrum k-distribution methods) for all but the most extreme situations.

Acknowledgements

The authors gratefully acknowledge the financial support of the National Science Foundation under contract CTS-0112423.

References

[1] Lacis AA, Oinas V. A description of the correlated-k distribution method for modeling nongray gaseous absorption, thermal emission, and multiple scattering in vertically inhomogeneous atmospheres. J Geophys Res 1991;96(D5): 9027–63.
[2] Goody RM, Yung YL. Atmospheric radiation—theoretical basis, 2nd ed. New York: Oxford University Press; 1989.
[3] Goody RM, West R, Chen L, Crisp D. The correlated k method for radiation calculations in nonhomogeneous atmospheres. JQSRT 1989;42:539–50.
[4] Fu Q, Liou KN. On the correlated k-distribution method for radiative transfer in nonhomogeneous atmospheres. J Atmos Sci 1992;49(22):2139–56.
[5] Modest MF, Zhang H. The full-spectrum correlated-k distribution for thermal radiation from molecular gas—particulate mixtures. ASME J Heat Transfer 2002;124(1):30–8.

[6] Modest MF. Narrow-band and full-spectrum k-distributions for radiative heat transfer—correlated-k vs. scaling approximation. JQSRT 2003;76(1):69–83.
[7] Modest MF. Radiative heat transfer, 2nd ed. New York: Academic Press; 2003.
[8] Rothman LS, Rinsland CP, Goldman A, Massie ST, Edwards DP, Flaud J-M, Perrin A, Camy-Peyret C, Dana V, Mandin J-Y, Schroeder J, McCann A, Gamache RR, Wattson RB, Yoshino K, Chance KV, Jucks KW, Brown LR, Nemtchinov V, Varanasi P. The HITRAN molecular spectroscopic database and HAWKS (HITRAN Atmospheric Workstation): 1996 edition. JQSRT 1998;60:665–710.
[9] Rothman LS, Camy-Peyret C, Flaud J-M, Gamache RR, Goldman A, Goorvitch D, Hawkins RL, Schroeder J, Selby JEA, Wattson RB. HITEMP, the high-temperature molecular spectroscopic database 2000, available through http://www.hitran.com.
[10] Zhang H, Modest MF. Scalable multi-group full-spectrum correlated-k distributions for radiative heat transfer. ASME J Heat Transfer 2003;125(3):454–61.
[11] Wang A, Modest MF. High-accuracy, compact database of narrow-band k-distributions for water vapor and carbon dioxide in Mengüc, MP, and Selçuk, N. (Eds.) Proceedings of the ICHMT 4th International Symposium on Radiative Transfer, Istanbul, Turkey, 2004.
[12] Taine J, Soufiani A. Gas IR radiative properties: from spectroscopic data to approximate models. In: Advances in heat transfer, vol. 33. New York: Academic Press; 1999. p. 295–414.
[13] Solovjov V, Webb BW. SLW modeling of radiative transfer in multicomponent gas mixtures. JQSRT 2000;65: 655–72.
[14] Domoto GA. Frequency integration for radiative transfer problems involving homogeneous non-gray gases: the inverse transmission function. JQSRT 1974;14:935–42.
[15] Chang H, Charalampopoulos TT. Determination of the wavelength dependence of refractive indices of flame soot. Proc R Soc (London) A 1990;430:577–91.
[16] van de Hulst HC. Light scattering by small particles. New York: Wiley; 1957 (also New York: Dover Publications; 1981).